Acta Crystallographica Section D
Biological Crystallography
ISSN 0907-4449

Polarization-resolved second-harmonic generation microscopy as a method to visualize protein-crystal domains

Emma L. DeWalt,‡ Victoria J. Begue,‡ Judith A. Ronau, Shane Z. Sullivan, Chittaranjan Das and Garth J. Simpson*

Department of Chemistry, Purdue University, 560 Oval Drive, West Lafayette, IN 47907-2084, USA

‡ These authors contributed equally to this work.

Correspondence e-mail: gsimpson@purdue.edu

Received 8 August 2012
Accepted 10 October 2012

Polarization-resolved second-harmonic generation (PR-SHG) microscopy is described and applied to identify the presence of multiple crystallographic domains within protein-crystal conglomerates, which was confirmed by synchrotron X-ray diffraction. Principal component analysis (PCA) of PR-SHG images resulted in principal component 2 (PC2) images with areas of contrasting negative and positive values for conglomerated crystals and PC2 images exhibiting uniformly positive or uniformly negative values for single crystals. Qualitative assessment of PC2 images allowed the identification of domains of different internal ordering within protein-crystal samples as well as differentiation between multi-domain conglomerated crystals and single crystals. PR-SHG assessments of crystalline domains were in good agreement with spatially resolved synchrotron X-ray diffraction measurements. These results have implications for improving the productive throughput of protein structure determination through early identification of multi-domain crystals.

1. Introduction

X-ray crystallography has become the method of choice for obtaining high-resolution protein structures, with over 70 000 protein structures solved by X-ray diffraction deposited in the Protein Data Bank (PDB) [compared with other techniques such as NMR and electron microscopy (EM), which together have contributed ~10 000 protein structures; http://www.pdb.org]. Despite advances in protein X-ray crystallographic techniques, predicting the diffraction quality of a crystal remains a challenge. Only a limited number of methods have been proposed for determining crystal quality prior to diffraction, including analysis of the birefringent properties of protein crystals and low-intensity X-ray diffraction prior to synchrotron X-ray diffraction (Watanabe, 2005; Owen & Garman, 2005). The lack of a reliable bench-top method for rapidly predicting crystal quality adds considerable time and expense to structure-determination efforts, since poorly diffracting low-quality crystals are often only identified as such after crystal harvesting and diffraction analysis by synchrotron-radiation X-ray diffraction (Lunde *et al.*, 2005; Vernede *et al.*, 2006; Groves *et al.*, 2007; Garcia-Caballero *et al.*, 2011). During crystal growth, multiple crystals can grow together in non-specific orientations and can complicate diffraction analysis, often resulting in poor quality of the structural data (Dauter, 2003; Borshchevskiy *et al.*, 2010; Boudjemline *et al.*, 2008; Garcia-Caballero *et al.*, 2011; Yeates & Fam, 1999). Crystalline samples with multiple domains are not always easily identifiable by bright-field imaging, especially for the specific case of twinning. Consequently, rapid and nondestructive identification of crystalline domains could significantly improve the

productive throughput of synchrotron facilities (Chayen & Saridakis, 2008; Santarsiero *et al.*, 2002; Walter *et al.*, 2003; Chayen, 2003; Bergfors, 2003; Stojanoff *et al.*, 2011; Kisselman *et al.*, 2011).

Recently, second-harmonic generation (SHG) microscopy, or second-order nonlinear imaging of chiral crystals (SONICC), has emerged as a complementary method for crystal detection (Kissick *et al.*, 2010; Wampler *et al.*, 2008; Hall & Simpson, 2010) and may have attractive properties for the identification of crystalline domains. SHG is a nonlinear optical process that is exquisitely sensitive to internal order. It is symmetry-forbidden in centrosymmetric media, and consequently amorphous liquids and glasses, solvated molecules and most achiral crystals generate no coherent SHG (Boyd, 2003). However, all crystals of natural proteins must adopt noncentrosymmetric lattices by nature of their intrinsic chirality, the large majority of which are symmetry-allowed for SHG (Shen, 1984; Gualtieri *et al.*, 2008; Perry *et al.*, 2005). As a result, SHG microscopy has been shown to produce higher contrast than common alternative methods such as birefringence, intrinsic ultraviolet fluorescence and trace fluorescence labeling (Kissick *et al.*, 2010; Haupert & Simpson, 2011).

The same selectivity for orientation and order manifests itself in the polarization-dependence of SHG. Owing to its coherent nature, the emerging polarization state of SHG generated from the sample is highly dependent on both the polarization state of the incident light as well as the symmetry and orientation of the crystal (Haupert & Simpson, 2011; Boyd, 2003; Simpson *et al.*, 2005). The polarization-dependent tensor describing SHG has up to 18 unique tensor elements defining its orientation and polarization-dependent response, compared with just three for linear optics (*i.e.* the three principal refractive indices; Hubbard, 1995; Azzam & Bashara, 1988). Consequently, a significantly greater amount of information is available from detailed nonlinear optical polarization measurements and analysis relative to analogous linear effects such as birefringence.

In this study, instrumentation and algorithms for polarization-resolved SHG (PR-SHG) microscopy with principal component analysis (PCA) were developed to assess the merits of SHG for crystal-domain detection. PR-SHG measurements of monolayers at interfaces have previously been shown to enable discrimination between samples with similar nonlinear optical properties (Begue, Everly *et al.*, 2009; Begue & Simpson, 2010; Begue, Moad *et al.*, 2009). Further, polarization-dependent SHG microscopy has a rich history of enabling structural and orientational studies (Psilodimitrakopoulos *et al.*, 2010; Amat-Roldan *et al.*, 2010; Chang *et al.*, 2011; Latour *et al.*, 2012; Duboisset *et al.*, 2012; Stoller *et al.*, 2002; Mansfield *et al.*, 2007; Nucciotti *et al.*, 2009; Filippidis *et al.*, 2009; Madden *et al.*, 2011; Tuer *et al.*, 2011; Brideau & Stys, 2012). PCA offers the advantages of simplicity, generality and the absence of required training when extracting the core features of high-dimensional data. The central goal of PCA is to capture the greatest amount of variance within a multidimensional data set by extracting a series of orthogonal factors (eigenvectors) that reduce the information-carrying dimensionality of the data set from many to only a few. The eigenvalues are sorted by descending order and the corresponding eigenvector of greatest value explains the largest variance of the data set, termed the first principal component (PC1; Varmuza, 2009; Hotelling, 1933; Wold *et al.*, 1987; Moore, 1981). The second principal component (PC2) is orthogonal to PC1 and accounts for the largest variance not captured by PC1, and so on (Varmuza, 2009).

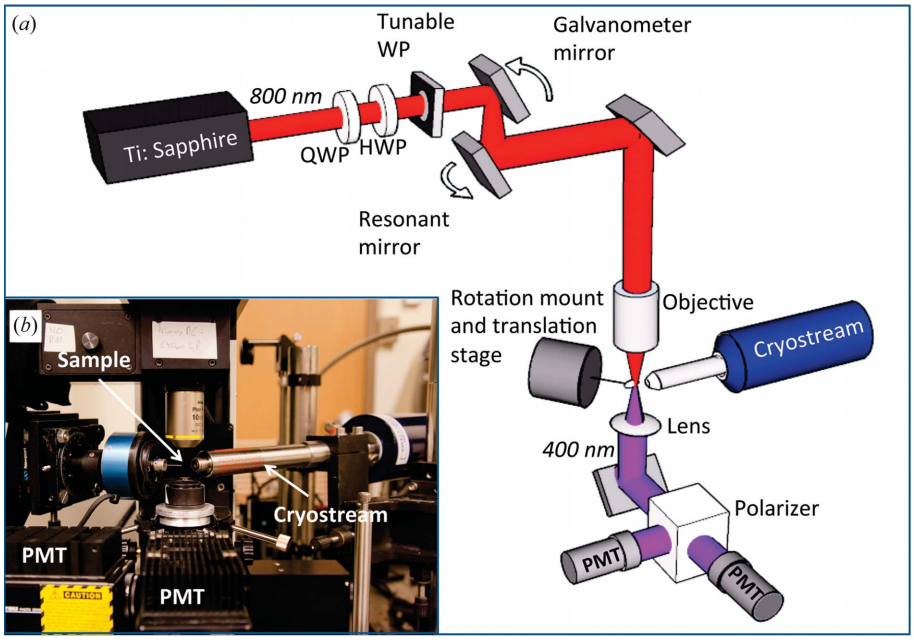

Figure 1
(*a*) An instrument schematic and (*b*) a photograph of the PR-SHG microscope (QWP, quarter-wave plate; HWP, half-wave plate; PMT, photomultiplier tube; tunable WP, tunable wave plate).

The potential for PCA of PR-SHG images was explored as a means of mining polarization-dependent SHG microscopy measurements to determine the presence of multiple domains in a crystalline sample. Validation of domain detection was performed by synchrotron X-ray diffraction raster imaging using a tightly collimated X-ray 'mini-beam' (Hilgart *et al.*, 2011; Cherezov *et al.*, 2009). PR-SHG microscopy was performed on cryogenic looped crystalline samples to enable direct comparison with synchrotron diffraction measurements. However, this method should also be applicable to samples in crystallization trays, as the conventional SHG microscopy instrumentation used for protein crystal detection is already optimized for routine screening within 96-well crystallization trays (Kissick *et al.*, 2010; Haupert & Simpson, 2011).

2. Methods

2.1. Protein crystallization

For crystallization, purified phenylalanine hydroxylase from *Chromobacterium violaceum* (cPAH) was concentrated to 10 mg ml^{-1} in a solution of 5 m*M* HEPES pH 7.4. Crystals of cPAH were obtained at ambient temperature utilizing hanging-drop vapor diffusion from solution No. 43 of the PEG/Ion 2 screen from Hampton Research [0.1 *M* Na HEPES pH 7.0, 0.01 *M* magnesium chloride hexahydrate, 0.005 *M* nickel(II) chloride hexahydrate, 15%(*w*/*v*) PEG 3350] with 8.3 m*M* hexammine cobalt(III) chloride and 8.3 m*M* guanidine hydrochloride as additives. Crystals of cPAH were grown *via* seeding using seeds (crushed crystals) of the wild-type protein. The total drop size was 5 µl (2 µl protein solution, 2 µl reservoir solution, 0.4 µl of each additive and 0.2 µl seeding solution). The described crystallization conditions are known to produce crystals of *P*1 symmetry (PDB entry 3tcy; J. A. Ronau, M. M. Abu-Omar & C. Das, submitted work). cPAH crystals were cooled in 25% ethylene glycol and maintained at cryogenic temperature for the duration of the experiment. Several loops that contained crystalline conglomerates were selected for PR-SHG imaging, as well as loops that appeared to contain single crystals.

2.2. PR-SHG imaging

The basic SHG microscopy instrument used for SONICC has been described previously and was originally designed for compatibility with 96-well plate screening at room temperature (Haupert & Simpson, 2011; Kissick *et al.*, 2010). Modifications were made to an existing SONICC instrument to allow compatibility with cryogenic looped samples, and an instrument schematic and photograph are shown in Fig. 1. Specific modifications include the addition of a rotation mount and miniature motorized translation stage (μ-Glide, Rigaku), which allowed rotation and fine *XYZ* positioning of looped crystals, and the installation of a 600 series Oxford Cryostream, which maintained the looped protein crystals at 100 K during imaging. An 80 MHz Tsunami Ti:Sapphire laser (Spectra Physics) provided the incident beam and SHG images were acquired with an incident wavelength of 800 nm and 75 mW average power at the sample. The beam was scanned with a slow-axis galvanometer mirror and a fast-axis resonant mirror. A 10× objective with a 1.6 cm working distance (Nikon, numerical aperture of 0.3) was used to focus the incident beam onto the sample. SHG images of the crystals were acquired at six different input polarizations by rotating a half-wave plate (HWP) and a quarter-wave plate (QWP) to produce horizontal (H), vertical (V), +45°, −45°, right-circular (RC) and left-circular (LC) polarizations. A wave plate independently tunable in both phase retardance and fast-axis orientation angle (Alphalas) was also included after the HWP and QWP in order to correct for the changes in polarization induced by the entire microscope beam path through to the objective. The SHG signal generated at the sample was collected in the transmitted direction with a 25.4 mm spherical lens and was separated by a Glan–Taylor polarizer into its horizontal and vertical components, which were then measured independently and simultaneously with two photomultiplier tubes (PMTs) (Hamamatsu). Bright-field images were acquired for each loop prior to SHG imaging. Although video-rate bright-field imaging was affected by thermal gradients under the cryogenic temperatures used, SHG images were acquired over a period of ∼30 s and image distortion was not observed.

2.3. PCA of PR-SHG images

PCA of PR-SHG images was performed using *R* v.2.15 with the built-in PCA function (*princomp*). PCA separates multi-dimensional pooled data based on the intrinsic axes of greatest signal variance. In the present case, this variance can arise

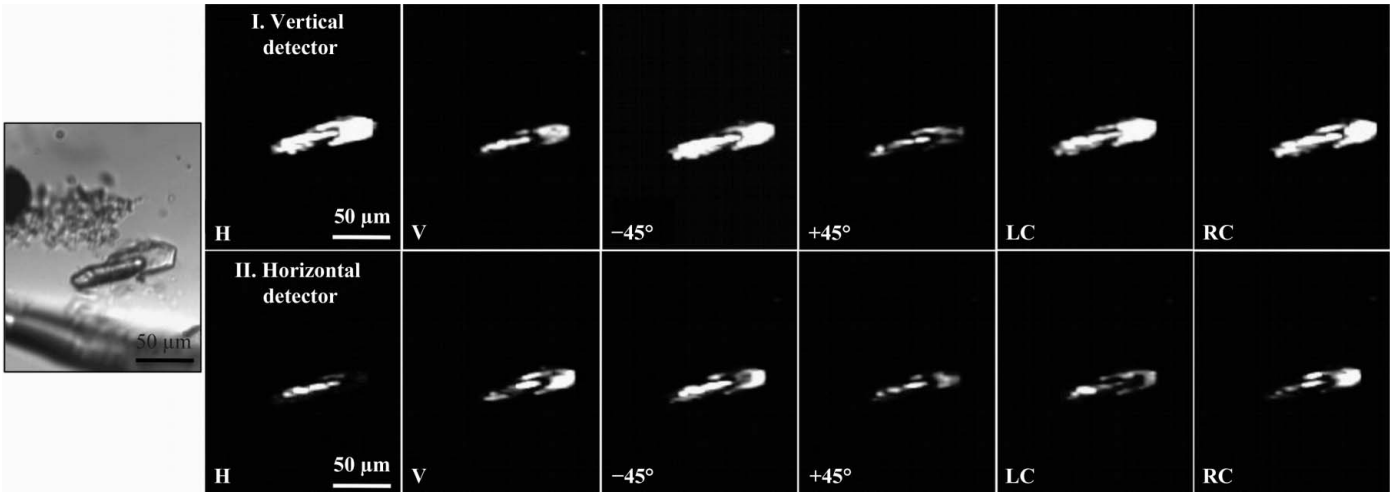

Figure 2
Set of PR-SHG images of a cPAH crystal conglomerate. Each image represents a unique combination of input and detected polarization. Row I corresponds to vertically polarized light at the detector and row II corresponds to horizontally polarized light at the detector. The respective input polarization for each image is given in the bottom left-hand corner of each SHG image (H, horizontally polarized; V, vertically polarized; + 45°, linearly polarized at + 45°; −45°, linearly polarized at −45°; RC, right-circularly polarized; LC, left-circularly polarized).

from changes in both the overall intensity as well as the polarization-dependence arising from differences in crystal orientation within the pooled data. In the present case for each given data set, 12 polarization-dependent measurements were obtained, each pixel of which corresponds to a single point in a 12-dimensional 'polarization space'. Including a diverse and representative set of crystals in many orientations within the pooled data set will increase the variance in the PCA owing to orientation effects, and more effectively identify the PC axes best capable of discriminating based on crystal orientation. Therefore, the combined data from eight samples were used in the PCA. Since PC axes are ranked by the corresponding variance, the first few axes provide the greatest separation, thereby reducing the overall dimensionality while retaining the majority of the polarization-dependent information content (PC1 and PC2 images are shown in Fig. 3).

2.4. Synchrotron diffraction measurements

Looped crystals were analyzed for synchrotron X-ray diffraction on beamline 23-ID-B at the Advanced Photon Source, Argonne National Laboratory after SHG imaging. Each loop was positioned in approximately the same orientation as in the original set of PR-SHG images and a raster grid with 5 μm squares was set up over the entire area of the crystalline sample. An X-ray beam with a wavelength of 0.979 Å was used for raster scans with tenfold attenuation, 1 s acquisition time and a sample-to-detector distance of 150 mm. A diffraction pattern was acquired for each square.

3. Results and discussion

A representative PR-SHG image stack is shown in Fig. 2 for a cPAH crystalline conglomerate. Substantial differences in overall intensity were observed for the different polarization combinations, consistent with a high sensitivity of SHG to polarization. Each pixel in the stack was described by a polarization-dependent vector to produce a 12-dimensional 'polarization space'. Although the full information of the measurements is contained within the complete polarization-dependent image stacks such as those shown in Fig. 2, the primary question of interest was whether more than one domain was present in the crystal. Generally, a material that exhibits uniform polarization-dependence is uniformly arranged throughout. Therefore, the presence of domains in the polarization-dependent SHG throughout a crystal should suggest a lower uniformity in the crystalline sample.

Using PCA for dimension reduction allowed the collective set of images to be concisely summarized by a small number of principal dimensions (in this case two) that carried the majority of the intrinsic information of the polarization-dependent responses. A representative set of results for the PCA of cPAH crystals and crystalline conglomerates is shown in Fig. 3, with PC1 images shown in row 2 and PC2 images shown in row 3 for six different cPAH crystalline samples (columns A–F).

All of the samples showed negative-valued PC1 images (row 2 of Fig. 3), with no meaningful separation between the different samples. Visual inspection of the raw images showed

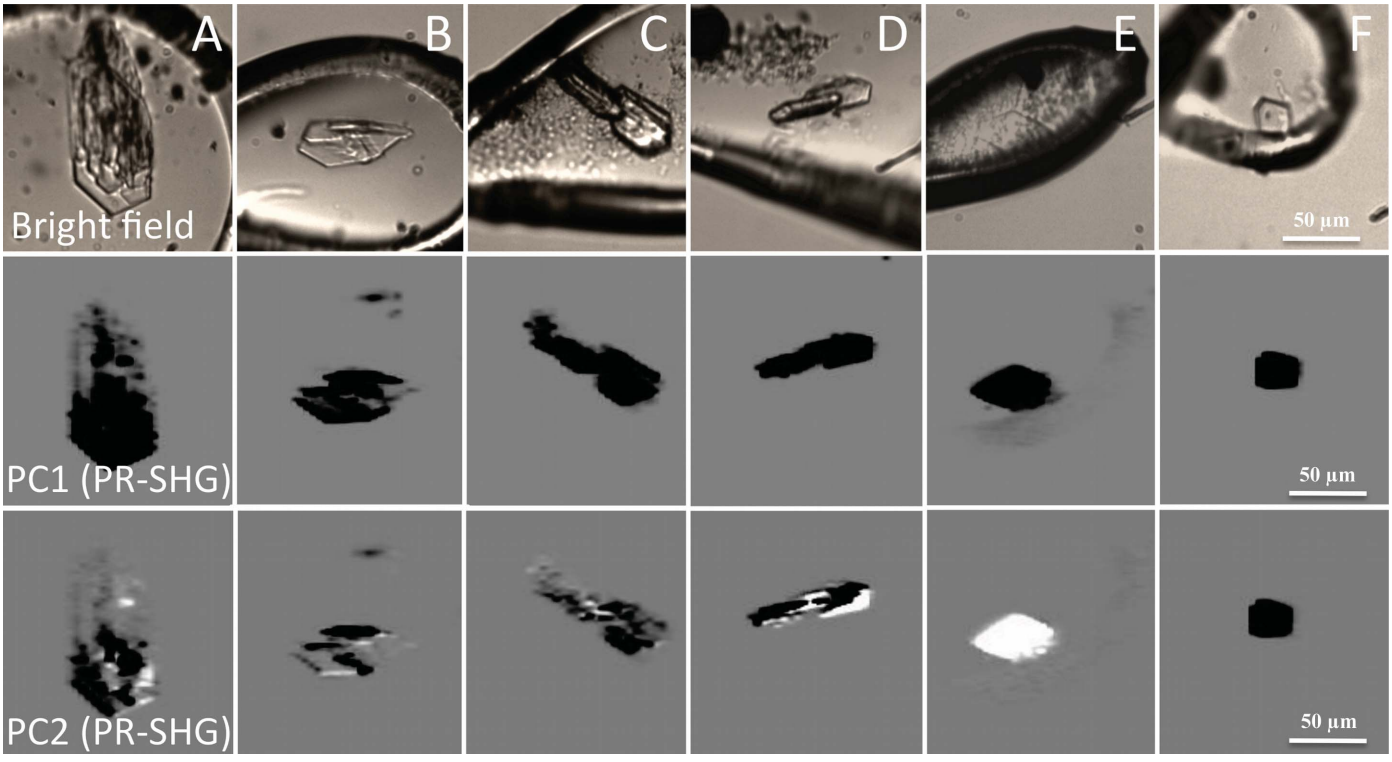

Figure 3
Bright-field images (row 1) and corresponding PC1 (row 2) and PC2 (row 3) images of PR-SHG images analyzed with PCA. Results for four cPAH crystalline conglomerates (columns A–D) and two apparently single pristine crystals (columns E and F) are shown. White regions correspond to large positive values and black regions correspond to large negative values.

that the majority of the variance in the images corresponded to crystal location. PC1 successfully distinguished the two regions corresponding to where the crystals are located and where they are not, showing large negative values in regions of crystals and near-zero values in regions that contained no crystals, producing in essence a domain map of sample location (Lee *et al.*, 2008; Loukas *et al.*, 2003). Consistent with this expectation, the elements defining PC1 contained 69% of the total signal variance. The absence of strong contrast in PC1 suggests that the overall SHG intensity alone is not a reliable indicator for discriminating between a single crystal and a multi-domain crystal, since it is dominated by effects that are unrelated to crystal orientation (*e.g.* the thickness of the crystal in a given pixel, the position within the focal volume, laser intensity, collection efficiency *etc.*).

In PC2, the images for the first four samples (A–D) exhibited substantial positive (white) and negative (black) contrasting regions within each crystallite, while samples E and F yielded uniformly positive and negative PC2 images, respectively. If it is assumed that crystal orientation represents the next most significant difference between the different locations within the crystals, PC2 should be dominated by differences in orientation and provide contrast for domain detection. PC2 contained 17% of the variance and collectively PC1 and PC2 comprise 86% of the total signal variance, with the higher principal coordinates largely dominated by additional subtle effects and measurement noise.

X-ray raster imaging was performed to assess the validity of these expectations. Fig. 4 shows diffraction patterns for three locations in sample F from Fig. 3. Consistent with the expectations from PCA for a single-domain crystal, all three diffraction patterns produced qualitatively similar X-ray diffraction patterns. In contrast, Fig. 5 shows diffraction patterns for four locations within a sample identified as a cPAH polycrystalline conglomerate based on PCA in Fig. 3(*d*). In this case, the four diffraction patterns appeared to differ from each other. Qualitatively similar results were obtained for all of the other crystals analyzed, with uniform single crystals identified by PCA corresponding to uniform diffraction patterns and multi-domain crystals producing distinctly different diffraction patterns as a function of location.

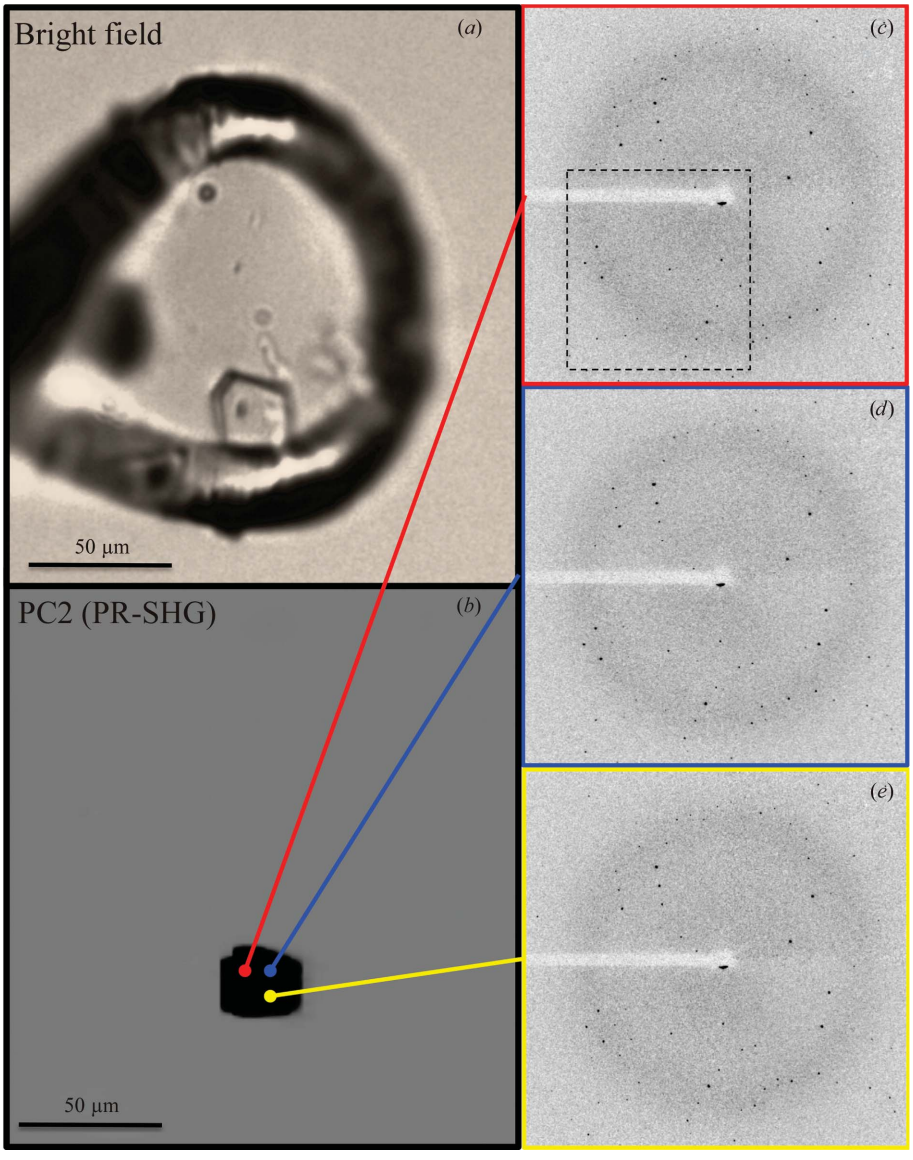

Figure 4
(*a*) Bright-field image and (*b*) PC2 SHG image for a single cPAH crystal. (*c*, *d*, *e*) Corresponding diffraction patterns for three separate locations within the crystal.

From visual bright-field inspection, the conglomerate in Fig. 5 appears to consist of only two domains. However, the presence of several regions of differing contrast in the PC2 image indicates that the conglomerate is more complicated than suggested by conventional optical imaging. Adjacent regions within the crystalline conglomerate that clearly differ in brightness in the PC2 image produced different X-ray diffraction patterns (Figs. 5*e* and 5*f*), while the bright-field image suggests that these two regions appear to be a single domain. The diffraction patterns presented in Figs. 5(*a*) and 5(*b*) also differ, indicating the presence of more than one crystalline domain. Fig. 6(*a*) shows an overlay of the three diffraction patterns from the single crystal and Fig. 6(*b*) shows the four diffraction patterns from the conglomerate. The different diffraction patterns were assigned different colors in the overlay (colors as shown in Figs. 4 and 5) and a

zoomed-in view is shown (area outlined by the black box in Figs. 4 and 5). Colors were chosen such that overlapping regions of the three (Fig. 6*a*) or four (Fig. 6*b*) colors added to give a white spot in the overlay. As shown in Fig. 6(*a*), white spots consistent with diffraction peaks uniformly appearing in multiple diffraction patterns were observed from samples exhibiting uniform contrast in PC2. The nearly identical diffraction pattern for three locations within the crystal suggests that the uniformity in the PC2 image indicates the presence of a single crystalline domain. Differences in the four diffraction patterns for the crystalline conglomerate from Fig. 5 were also clearly observed in Fig. 6(*b*), with individual red, blue, green and orange diffraction spots dominating the overlay and very few spots showing overlapping colors. The differences in the diffraction patterns confirm the presence of multiple crystalline domains, suggesting that the non-uniformity in the PC2 image is a reliable indication of the presence of more than one crystalline domain.

The PCA images present a single scalar value that depends nontrivially on crystallographic orientation, and consequently the value of PC2 should not necessarily indicate identical crystallographic orientations within multi-domain crystals. Prior studies suggest that it is reasonable to expect crystals of similar orientation to produce similar values from PCA (Begue & Simpson, 2010), but even subtle differences in orientation that are too small to enable discrimination by PCA could still yield distinct diffraction patterns. Consistent with these expectations, the diffraction patterns in Fig. 5 do not necessarily correspond to a single domain and the regions of similar contrast in Fig. 5 do not necessarily indicate identically oriented domains. Rather, this figure demonstrates that the crystalline sample contained several areas of differing contrast and sign in the PC2 image and that this sample also yielded non-uniform diffraction.

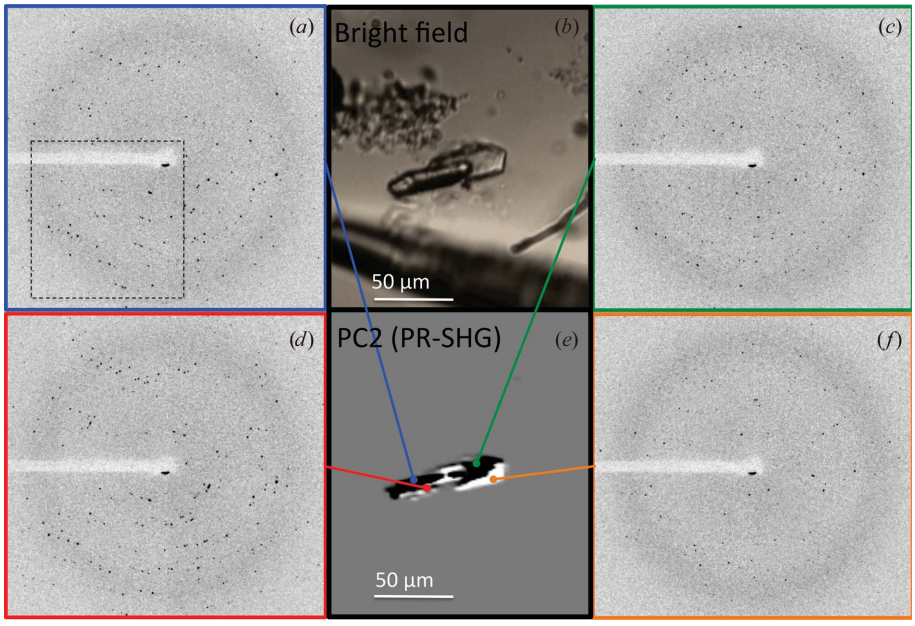

Figure 5
Bright-field image (*c*) and PC2 SHG image (*d*) for a cPAH crystal conglomerate. (*a*, *b*, *e*, *f*) Corresponding diffraction patterns for four separate locations within the crystalline conglomerate.

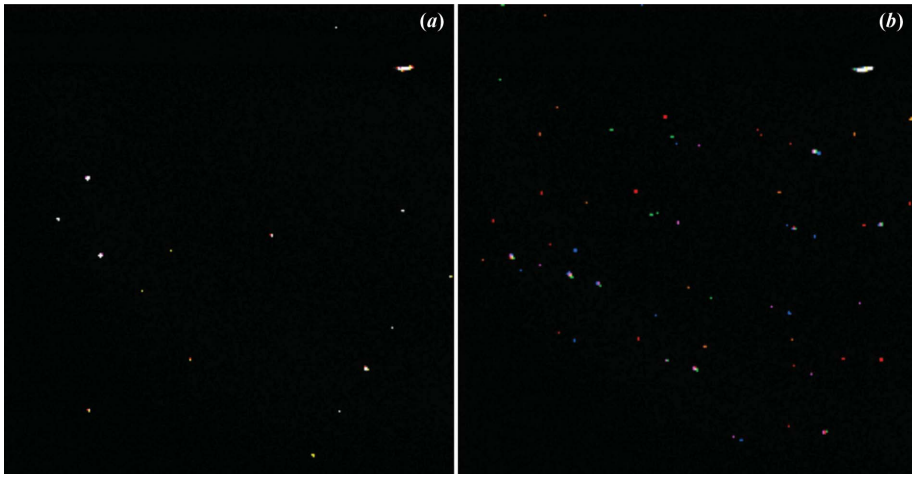

Figure 6
A zoomed-in overlay of a section of (*a*) the three diffraction patterns from Fig. 3 assigned their respective colors (red, blue and yellow) and (*b*) the four diffraction patterns from the crystalline sample from Fig. 4 assigned their respective colors (blue, red, green and orange). In both (*a*) and (*b*), white indicates overlapping diffraction spots between the individual diffraction patterns.

Although the PR-SHG measurements performed in this work were acquired for looped crystals to enable independent validation by X-ray diffraction, the greatest benefits are likely to be realised in the analysis of crystals still within the mother liquor prior to harvesting. The incorporation of PR-SHG measurements into routine screening of crystallization trays could allow the early identification of multi-domain crystals, such that time is not spent on crystallization procedures and synchrotron diffraction measurements that are unlikely to yield high-quality structures. Furthermore, the experimental modifications to instrumentation developed previously for plate-reading by SHG (Haupert & Simpson, 2011) involve only the addition of simple wave plates and polarizers. Consequently, this approach may provide a means of rapidly screening to select a subset of crystals that are most likely to produce single-crystal diffraction in subsequent X-ray analysis.

A potential drawback to this strategy is the sixfold increase in the measurement time compared with conventional screening by SHG microscopy (Kissick

et al., 2010) when using dual-polarization detection or the 12-fold increase when using a single detector. The incorporation of rapid polarization-modulation approaches into the instrumental design has the potential to decrease acquisition times as well as to reduce noise and to allow for better discrimination between domains (Begue & Simpson, 2010). Finally, although the combined results of only eight samples still enabled the identification of PC axes capable of effectively identifying multi-domain crystals in the present study, the ability of PCA of PR-SHG data to separate crystals based on orientation may improve further with a larger sampling of different crystal orientations. Most crystallization droplets contain multiple crystallites, such that the PCA could be performed from the combined polarization-dependent data acquired either within a single droplet or from a larger pooled data set from crystals in multiple droplets of the same crystal space group.

Although these collective results indicate the potential promise of the application of PR-SHG microscopy for the detection of unique crystallographic domains, it should be noted that these collective data were acquired for only one type of protein crystal. The broader utility of the approach remains to be tested through systematic studies of many protein crystals by combined PR-SHG microscopy and spatially resolved synchrotron X-ray diffraction. Nevertheless, the initial results from this study suggest that it is possible to identify polycrystalline samples that could complicate subsequent diffraction analysis at early stages in the crystal-screening process. Furthermore, it may be possible through PR-SHG microscopy to localize the diffraction analysis to single domains to reduce complications in indexing and subsequent structure determination of conglomerated or twinned crystals. Confirmation of PR-SHG microscopy for this application will be the subject of further study.

4. Conclusions

PR-SHG microscopy analyzed by PCA was found to be a rapid and nonperturbative technique compatible with X-ray crystallography for identifying polycrystalline conglomerates. These measurements take advantage of the coherent nature of SHG, in which the frequency-doubled light emerges in a well defined polarization state dependent on the incident driving polarization, the nonlinear optical properties of the crystal and the crystallographic orientation within the laboratory frame. PR-SHG microscopy was shown to reliably distinguish multi-domain crystalline samples from single crystals. Identification of differences in crystal orientation are demonstrated with the intention of moving towards the rapid and reliable all-optical identification of crystals that are likely to provide the single-domain diffraction typically associated with high-resolution protein structures and the selection of promising regions for diffraction within crystalline conglomerates or other types of multi-domain crystals that otherwise would have resulted in poor diffraction data.

The authors gratefully acknowledge support from NIH Grant No. R01GM-103401-3 from the National Institute of General Medical Science (NIGMS) and support from Eli Lilly and Co. from the Research Awards Program. The authors also wish to acknowledge the GM/CA CAT beamline (23-ID-B) at the Advanced Photon Source, Argonne National Laboratory where synchrotron X-ray diffraction measurements were performed, and Ruslan (Nukri) Sanishvili for hosting our beam time. Use of the Advanced Photon Source, an Office of Science User Facility operated for the US Department of Energy (DOE) Office of Science by Argonne National Laboratory, was supported by the US DOE under Contract No. DE-AC02-06CH11357. We would also like to acknowledge Scott J. Toth for providing photography of the SHG microscope.

References

Amat-Roldan, I., Psilodimitrakopoulos, S., Loza-Alvarez, P. & Artigas, D. (2010). *Opt. Express*, **18**, 17209–17219.
Azzam, R. M. A. & Bashara, N. M. (1988). *Ellipsometry and Polarized Light.* Amsterdam: North Holland.
Begue, N. J., Everly, R. M., Hall, V. J., Haupert, L. & Simpson, G. J. (2009). *J. Phys. Chem. C*, **113**, 10166–10175.
Begue, N. J., Moad, A. J. & Simpson, G. J. (2009). *J. Phys. Chem. C*, **113**, 10158–10165.
Begue, N. J. & Simpson, G. J. (2010). *Anal. Chem.* **82**, 559–566.
Bergfors, T. (2003). *J. Struct. Biol.* **142**, 66–76.
Borshchevskiy, V., Efremov, R., Moiseeva, E., Büldt, G. & Gordeliy, V. (2010). *Acta Cryst.* D**66**, 26–32.
Boudjemline, A., Clarke, D. T., Freeman, N. J., Nicholson, J. M. & Jones, G. R. (2008). *J. Appl. Cryst.* **41**, 523–530.
Boyd, R. W. (2003). *Nonlinear Optics*, 2nd ed. San Diego: Academic Press.
Brideau, C. & Stys, P. K. (2012). *Proc. SPIE*, **8226**, 82263A.
Chang, Y., Wei, H., Jin, Y., Liu, H. & Deng, X. (2011). *Gen. Physiol. Biophys.* **30**, 175–185.
Chayen, N. E. (2003). *J. Struct. Funct. Genomics*, **4**, 115–120.
Chayen, N. E. & Saridakis, E. (2008). *Nature Methods*, **5**, 147–153.
Cherezov, V., Hanson, M. A., Griffith, M. T., Hilgart, M. C., Sanishvili, R., Nagarajan, V., Stepanov, S., Fischetti, R. F., Kuhn, P. & Stevens, R. C. (2009). *J. R. Soc. Interface*, **6**, S587–S597.
Dauter, Z. (2003). *Acta Cryst.* D**59**, 2004–2016.
Duboisset, J., Ait-Belkacem, D., Roche, M., Rigneault, H. & Brasselet, S. (2012). *Phys. Rev. A*, **85**, 043829.
Filippidis, G., Troulinaki, K., Fotakis, C. & Tavernarakis, N. (2009). *Laser Phys.* **19**, 1475–1479.
Garcia-Caballero, A. *et al.* (2011). *Cryst. Growth Des.* **11**, 2112–2121.
Groves, M. R., Müller, I. B., Kreplin, X. & Müller-Dieckmann, J. (2007). *Acta Cryst.* D**63**, 526–535.
Gualtieri, E. J., Haupert, L. M. & Simpson, G. J. (2008). *Chem. Phys. Lett.* **465**, 167–174.
Hall, V. J. & Simpson, G. J. (2010). *J. Am. Chem. Soc.* **132**, 13598–13599.
Haupert, L. M. & Simpson, G. J. (2011). *Methods*, **55**, 379–386.
Hilgart, M. C., Sanishvili, R., Ogata, C. M., Becker, M., Venugopalan, N., Stepanov, S., Makarov, O., Smith, J. L. & Fischetti, R. F. (2011). *J. Synchrotron Rad.* **18**, 717–722.
Hotelling, H. (1933). *J. Educ. Psychol.* **24**, 417–441.
Hubbard, A. T. (1995). *The Handbook of Surface Imaging and Visualization.* Boca Raton: CRC Press.
Kisselman, G., Qiu, W., Romanov, V., Thompson, C. M., Lam, R., Battaile, K. P., Pai, E. F. & Chirgadze, N. Y. (2011). *Acta Cryst.* D**67**, 533–539.

Kissick, D. J., Gualtieri, E. J., Simpson, G. J. & Cherezov, V. (2010). *Anal. Chem.* **82**, 491–497.
Latour, G., Gusachenko, I., Kowalczuk, L., Lamarre, I. & Schanne-Klein, M. C. (2012). *Biomed. Opt. Express*, **3**, 1–15.
Lee, J. L. S., Gilmore, I. S. & Seah, M. P. (2008). *Surf. Interface Anal.* **40**, 1–14.
Loukas, C. G., Wilson, G. D., Vojnovic, B. & Linney, A. (2003). *Cytometry A*, **55**, 30–42.
Lunde, C. S., Rouhani, S., Remis, J. P., Ruzin, S. E., Ernst, J. A. & Glaeser, R. M. (2005). *J. Appl. Cryst.* **38**, 1031–1034.
Madden, J. T., Hall, V. J. & Simpson, G. J. (2011). *Analyst*, **136**, 652–662.
Mansfield, J., Winlove, C. P., Moger, J., Knapp, K. & Matcher, S. (2007). *Proc. SPIE*, **6442**, 6442T.
Moore, B. C. (1981). *IEEE Trans. Autom. Control*, **26**, 17–32.
Nucciotti, V., Stringari, C., Sacconi, L., Vanzi, F., Linari, M., Piazzesi, G., Lombardi, V. & Pavone, F. S. (2009). *Proc. SPIE*, **7183**, 71831W.
Owen, R. L. & Garman, E. (2005). *Acta Cryst.* D**61**, 130–140.
Perry, J. M., Moad, A. J., Begue, N. J., Wampler, R. D. & Simpson, G. J. (2005). *J. Phys. Chem. B*, **109**, 20009–20026.
Psilodimitrakopoulos, S., Amat-Roldan, I., Loza-Alvarez, P. & Artigas, D. (2010). *J. Opt.* **12**, 084007.
Santarsiero, B. D., Yegian, D. T., Lee, C. C., Spraggon, G., Gu, J., Scheibe, D., Uber, D. C., Cornell, E. W., Nordmeyer, R. A., Kolbe, W. F., Jin, J., Jones, A. L., Jaklevic, J. M., Schultz, P. G. & Stevens, R. C. (2002). *J. Appl. Cryst.* **35**, 278–281.
Shen, Y. R. (1984). *The Principles of Nonlinear Optics*, 1st ed. Hoboken: Wiley-Interscience.
Simpson, G. J., Dailey, C. A., Plocinik, R. M., Moad, A. J., Polizzi, M. A. & Everly, R. M. (2005). *Anal. Chem.* **77**, 215–224.
Stojanoff, V., Jakoncic, J., Oren, D. A., Nagarajan, V., Navarro Poulsen, J.-C., Adams-Cioaba, M. A., Bergfors, T. & Sommer, M. O. A. (2011). *Acta Cryst.* F**67**, 971–975.
Stoller, P., Kim, B.-M., Rubenchik, A. M., Reiser, K. M. & Da Silva, L. B. (2002). *J. Biomed. Opt.* **7**, 205–214.
Tuer, A. E., Krouglov, S., Prent, N., Cisek, R., Sandkuijl, D., Yasufuku, K., Wilson, B. C. & Barzda, V. (2011). *J. Phys. Chem. B*, **115**, 12759–12769.
Varmuza, K. F. P. (2009). *Introduction to Multivariate Statistical Analysis in Chemometrics.* Boca Raton: CRC Press.
Vernede, X., Lavault, B., Ohana, J., Nurizzo, D., Joly, J., Jacquamet, L., Felisaz, F., Cipriani, F. & Bourgeois, D. (2006). *Acta Cryst.* D**62**, 253–261.
Walter, T. S., Diprose, J., Brown, J., Pickford, M., Owens, R. J., Stuart, D. I. & Harlos, K. (2003). *J. Appl. Cryst.* **36**, 308–314.
Wampler, R. D., Kissick, D. J., Dehen, C. J., Gualtieri, E. J., Grey, J. L., Wang, H. F., Thompson, D. H., Cheng, J. X. & Simpson, G. J. (2008). *J. Am. Chem. Soc.* **130**, 14076–14077.
Watanabe, N. (2005). *J. Appl. Cryst.* **38**, 396–397.
Wold, S., Esbensen, K. & Geladi, P. (1987). *Chemometrics Intell. Lab. Syst.* **2**, 37–52.
Yeates, T. O. & Fam, B. C. (1999). *Structure*, **7**, R25–R29.